RESEARCH PAPER

3-acetyl -11-keto-beta-boswellic acid: A novel approach to target the HMGB1 pathway in the gut-brain axis of diabetes mellitus-induced alzheimer's disease via PPAR-γ

Hari Priya. S[1], Dr. K. Gayathiri [2*], Dr. V. Chitra[3], Dr. K. Gowri[4]

[1,2*,3,4]Department Of Pharmacology, SRM College Of Pharmacy, SRM Institute of Science and Technology, Kattankulathur, Chengalpattu, 603203, Tamil Nadu, India

ABSTRACT

Alzheimer's disease (AD) and type 2 diabetes mellitus (T2DM) share common pathological features, including insulin resistance, chronic inflammation, and gut-brain axis (GBA) dysfunction, which contribute to neurodegeneration. High-mobility group box 1 (HMGB1), a pro-inflammatory protein elevated in both conditions, activates TLR4 and RAGE receptors, triggering NF-κB-mediated cytokine release and neuronal damage. Peroxisome proliferator-activated receptor gamma (PPAR-γ) counteracts HMGB1-induced inflammation by inhibiting NF-κB signaling. 3-Acetyl-11-keto-β-boswellic acid (3-AKBA), a bioactive compound from Boswellia serrata, exhibits anti-inflammatory and neuroprotective effects by activating PPAR-γ, reducing oxidative stress, and improving cognitive function in diabetic AD models. This study explores the therapeutic potential of 3-AKBA in modulating the HMGB1–PPAR-γ axis, proposing it as a promising candidate to mitigate inflammation-driven neurodegeneration in diabetes-associated AD.

Keywords: Alzheimer's disease, Diabetes mellitus, HMGB1, PPAR-γ, 3-AKBA, Neuroinflammation, Gut-brain axis, NF-κB, Neurodegeneration.

How to cite this article: Priya.S H, Gayathiri K, Chitra V, 3-acetyl -11-keto-beta-boswellic acid: A novel approach to target the HMGB1 pathway in the gut-brain axis of diabetes mellitus-induced alzheimer's disease via PPAR-γ. Int J Drug Deliv Technol. 2026;16(9s): 755-780; Doi: 10.25258/Ijddt.16.9s.79.

Source of support: Nil

Conflict of interest: None

INTRODUCTION

Diabetes mellitus (DM) is a chronic metabolic disorder characterized by persistent hyperglycemia due to inadequate insulin production or impaired insulin action. In 2021, around 537 million adults (10.5% globally) were affected, with type 2 DM (T2DM) accounting for nearly 90% of cases [1]. This number is projected to rise to 783 million by 2045. DM is the seventh leading cause of death and imposes a major economic burden, with annual healthcare costs around US$760 billion. Common symptoms include polyuria, fatigue, weight loss, and recurrent infections. Long-term complications mainly involve cardiovascular diseases (75% of DM-related deaths), stroke, peripheral artery disease, and neurodegenerative conditions such as Alzheimer's disease (AD) [1].

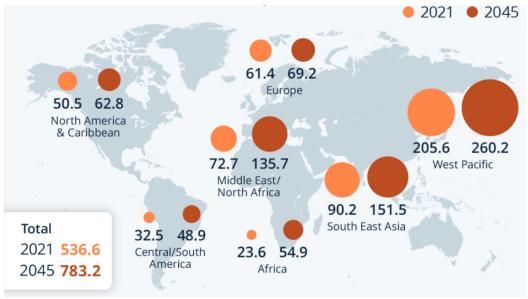

Fig 1: Prevalence of Diabetes Mellitus

Neurological complications affect 60–70% of DM patients and include diabetic neuropathy, erectile dysfunction, and cognitive decline. Insulin resistance contributes to AD through disrupted insulin signaling pathways involving IRS-1/2 and PI3K, which are crucial for memory, synaptic function, and protection against

amyloid-beta (Aβ) toxicity. These disruptions also affect neurotransmitter systems via GABA, AMPA, and NMDA receptors [2,3]. The HMGB1 protein, a key inflammatory mediator, is linked to gut-brain axis (GBA) dysfunction in DM [4,5]. Chronic hyperglycemia leads to gut dysbiosis, leaky gut, and systemic inflammation, impairing brain function. Severe complications like DKA, HHS, and hypoglycemia further highlight the need for therapies targeting both metabolic and neurological aspects of DM [6].

1.1 Therapeutic Potential of Targeting the Gut-Brain Axis in Alzheimer’s Disease

Alzheimer's disease (AD) is a progressive neurodegenerative disorder and the leading cause of dementia, accounting for 60–70% of cases and affecting over 27 million people worldwide [7,8]. Characterized by cognitive decline, memory loss, and disorientation, AD is marked by amyloid plaques and neurofibrillary tangles. Risk factors include depression, hypertension, head trauma, and cerebral amyloid angiopathy. The amyloid hypothesis suggests that amyloid beta (Aβ) accumulation, influenced by genes like APP on chromosome 21 and the ApoE4 variant, drives disease progression [9,10].

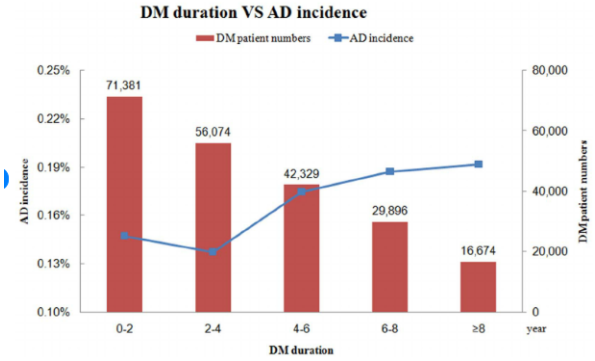

Fig 2: Prevalence of Diabetic patients with Alzheimer.

Recent research highlights the role of the gut-brain axis (GBA) in AD, involving communication through the vagus nerve, HPA axis, immune signaling, and microbial metabolites [11,12]. Gut microbiota influences neurotransmitters like GABA and serotonin, with *Lactobacillus* and *Bifidobacterium* playing key roles. Dysbiosis leads to harmful compounds like amyloids and lipopolysaccharides (LPS), causing microglial activation and neuroinflammation [13]. A leaky gut allows toxins into circulation, worsening brain inflammation. Microbial byproducts impact cognition via immune cells and vagal pathways [14,15]. Altered bile acids and HMGB1 pathway dysregulation especially in diabetes-related AD further link gut health to neurodegeneration [16,17]. These insights support microbiota-targeted therapies as promising interventions to slow AD progression.

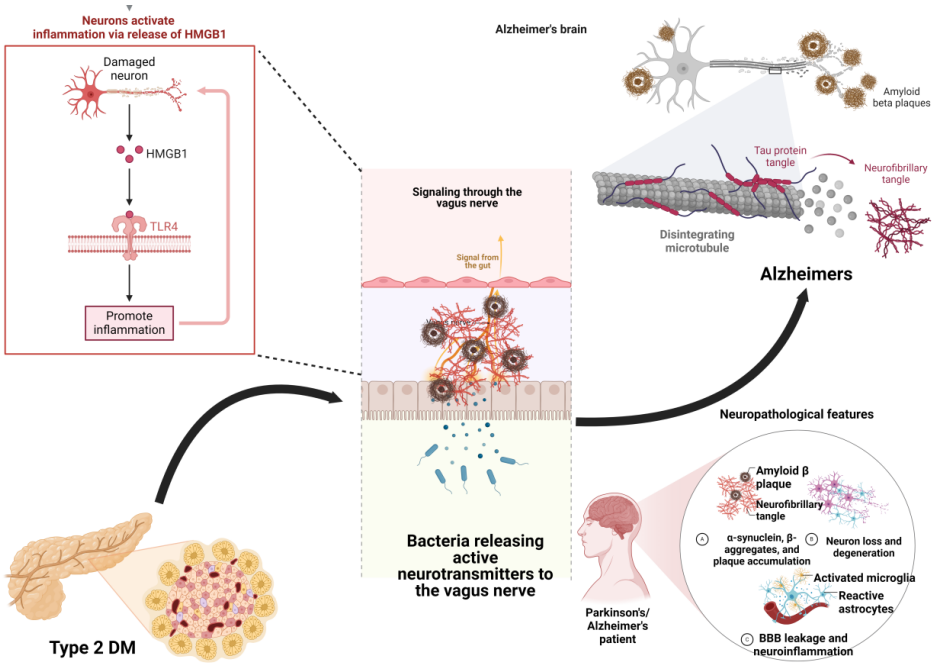

Fig 3: HMGB1 pathway interlinking diabetes and AD through GBA

1.2 PPAR-γ Mediated Modulation of HMGB1 Pathway by 3-AKBA in Alzheimer's Disease

The The HMGB1 pathway plays a critical role in inflammation, immune regulation, and neurodegeneration. HMGB1, a non-histone chromatin protein, interacts with receptors like TLR4 and RAGE, driving neuroinflammation in Alzheimer's disease (AD) [18–20]. Elevated HMGB1 levels in the brain and cerebrospinal fluid of AD patients, particularly in diabetes-associated AD, contribute to Aβ accumulation, neuronal damage, and cognitive decline through the HMGB1-RAGE-TLR4 axis [21–23]. It also links gut dysbiosis to systemic inflammation by disrupting the intestinal barrier, worsening AD pathology in conditions like T2DM via oxidative stress and immune dysfunction [22,23].

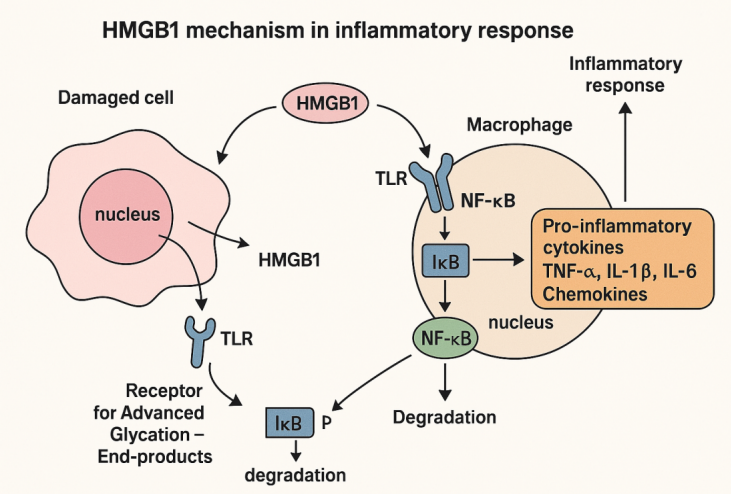

Figure 4: HMGB1 mechanism in Inflammatory response.

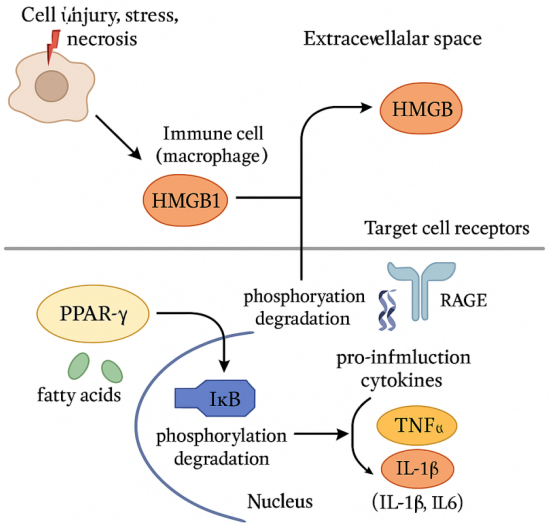

Fig 5: Activation of PPAR-γ and Inhibition of HMGB1 Pathway by PPAR-γ.

PPAR-γ, an anti-inflammatory nuclear receptor, counteracts HMGB1 signaling by inhibiting NF-κB and cytokine release, offering neuroprotection [24–27]. *3-Acetyl-11-keto-β-boswellic acid* (3-AKBA), derived from Boswellia serrata, activates PPAR-γ, suppressing NF-κB and MAPK pathways to reduce inflammation and oxidative stress [28–37]. Preclinical studies show that 3-AKBA improves memory, lowers Aβ levels, and reduces neuroinflammation and synaptic damage in AD models [38]. It also enhances cholinergic function by inhibiting AChE [39] and helps manage T2DM and insulin resistance [40]. This supports 3-AKBA's therapeutic potential in targeting HMGB1 via PPAR-γ activation to combat diabetes-induced neurodegeneration.

MATERIALS AND METHOD

2.1. Network Pharmacology

A network pharmacology approach was used to explore interactions between 3-AKBA and disease targets. Drug-related genes (Homo sapiens) were identified via SwissADME, while disease-associated genes were obtained from DisGeNET. Common targets were visualized using InteractiVenn and analyzed through STRING for PPI data. The resulting network was further visualized using Cytoscape to map disease-drug interactions.

2.2. In Silico Studies

In-silico analyses were performed to evaluate 3-AKBA's interactions and properties. Its 3D structure was optimized and docked with Homo sapiens protein targets using CB-DOCK2. Pharmacokinetic and ADMET properties were predicted via SwissADME and Protoxprediction. Molecular dynamics simulations using Schrödinger assessed the stability of ligand-protein complexes.

2.3. Procurement of 3-AKBA

3-AKBA was purchased in powder form. Then run it through HPLC for purity and quantity.

2.4. In-vitro Studies

2.4.1. Cytotoxicity Using Brine Shrimp Lethality Assay

Brine shrimp lethality assay was used to assess 3-AKBA toxicity. Nauplii were hatched in artificial seawater (35 g sea salt/L) under light at 25–30°C. 3-AKBA and standard (potassium dichromate) solutions were prepared in DMSO-water at 200–1000 µg/mL. Ten nauplii were exposed to each concentration, and mortality was recorded after 24 hours. LC_{50} was calculated using probit analysis [41, 42].

Calculation:

- Calculate the percentage of dead brine shrimp for each concentration as follows:

$$\text{Mortality Rate (\% of death)} = \frac{\text{Number of dead nauplii}}{\text{Total Number of nauplii}} \times 100$$

- LC50 Value: Calculate the LC50, plot the percentage of mortality versus concentration of 3-AKBA.

2.4.2. Antioxidant Assay

DPPH (2, 2-Diphenyl-1-picrylhydrazyl): DPPH assay was used to assess antioxidant activity of 3-AKBA. A 0.1 mM DPPH solution was prepared in methanol and stored at 4°C. 3-AKBA and ascorbic acid (standard) were diluted to 200–1000 µg/mL. 1 mL DPPH was added to each test tube, incubated in dark for 30 min, and absorbance was measured at 517 nm [43].

Calculation:

- This were calculated by using an equation:

$$\%\text{Radical Scavenging Activity (\% RSA)} = \frac{\text{Control} - \text{Sample}}{\text{Control}} \times 100$$

- Plot % inhibition and determine IC_{50}.

FRAP (Ferric Reducing Antioxidant Power): FRAP assay was performed to evaluate antioxidant activity of 3-AKBA. FRAP reagent was prepared by mixing acetate buffer, TPTZ, and $FeCl_3$ (10:1:1) and preheated to 37°C. 3-AKBA and ascorbic acid were diluted to 200–1000 µg/mL. 2.85 mL FRAP reagent and test solutions were incubated at 37°C for 30 min in dark. Absorbance was measured at 593 nm [44].

Calculation:

- Compare the absorbance of 3-AKBA with the standard (Ascorbic Acid).
- Plot % inhibition and determine IC_{50}.
- The antioxidant capacity of 3-AKBA is calculated by using the equation:

$$\%\text{ FRAP Activity (\%FA)} = \frac{\text{Control} - \text{Sample}}{\text{Control}} \times 100$$

2.4.3. Anti-inflammatory using Protein Denaturation Method

Protein denaturation assay was used to assess anti-inflammatory activity of 3-AKBA. Egg albumin solution (5 g/100 mL) was prepared. 3-AKBA and diclofenac were diluted to 200–1000 µg/mL. 2 mL of albumin and test/standard solutions were incubated at room temp (15–30 min), then at 70°C for 10 min. After cooling, absorbance was measured at 660 nm. Lower absorbance indicates stronger anti-inflammatory effect [45].

Calculation:

- The percentage of inhibition can be calculated using the formula:

$$\%\text{ Inhibition} = \frac{\text{Control} - \text{Sample}}{\text{Control}} \times 100$$

- This calculation will give the percentage of protein denaturation that was prevented by 3-AKBA (or any other tested compound).

Plot the percentage of inhibition and determine the IC_{50}. (The concentration required to inhibit 50% of the protein denaturation).

2.4.4 Hyperglycaemic Studies

Alpha-Amylase Assay Using Iodine Starch Method: Alpha-amylase inhibition assay was used to evaluate 3-AKBA's antidiabetic activity. 3-AKBA and acarbose were diluted to 200–1000 µg/mL. Each test tube received phosphate buffer, α-amylase, starch, and test solutions, then incubated at 37°C for 10 min. Iodine reagent was added to form a blue complex, followed by phosphate buffer. Absorbance was measured at 620 nm; higher absorbance indicates greater inhibition [46].

Calculation:

- The percentage inhibition can be calculated by using an equation:

$$\%\text{ Inhibition} = \frac{\text{Control} - \text{Sample}}{\text{Control}} \times 100$$

- Plot the inhibition percentage curve.
- Compare the inhibitory activity of 3-AKBA to Acarbose by determining the IC_{50} values (the concentration required to inhibit 50% of alpha-amylase activity).

Alpha-Glucosidase Assay: α-Glucosidase inhibition assay was performed to assess antidiabetic activity of 3-AKBA. Enzyme (1 U/mL) and 2% sucrose substrate were prepared. 3-AKBA and acarbose were diluted to 200–1000 µg/mL. Each tube received enzyme, test/standard drug, and sucrose, then incubated at 37°C for 10 min. DNS reagent was added to stop the reaction, followed by boiling for 5 min. Absorbance was measured at 540 nm; lower absorbance indicates higher inhibition [47].

Calculation:

- The percentage inhibition can be calculated by using an equation:

$$\%\text{ Inhibition} = \frac{\text{Control} - \text{Sample}}{\text{Control}} \times 100$$

- 3-AKBA's effect is compared with Acarbose to determine its potential as an α-glucosidase inhibitor.

Glucose Uptake Assay In Yeast Cells Using DNS: Glucose uptake by yeast assay was used to evaluate 3-AKBA's antidiabetic effect. Yeast was activated, washed, and resuspended. Test tubes received glucose (500 µL), yeast (300 µL), and 3-AKBA or metformin (200–1000 µg/mL). Samples were incubated at 37°C for 30 min, centrifuged, and supernatant mixed with DNS reagent. After boiling for 10 min at 90°C, absorbance

was measured at 540 nm. Lower absorbance indicates higher glucose uptake. [48].

Calculation:

- Calculate glucose uptake percentage using an equation:

$$\% \text{ Inhibition of Glucose uptake} = \frac{\text{Control} - \text{Sample}}{\text{Control}} \times 100$$

- Plot the graph for glucose uptake by comparing 3-AKBA and Metformin and determine IC_{50} (inhibits 50% of the glucose uptake activity).

2.4.5 Cell Line Study

Cell Viability Using MTT Assay: MTT assay was conducted on 3T3-L1 cells to evaluate cytotoxicity of 3-AKBA and pioglitazone. Cells were cultured in DMEM with 10% FBS and 1% antibiotics at 37°C, 5% CO_2. After seeding and 24–48 h incubation, cells were treated with test compounds for 24 h. MTT (5 mg/mL) was added, incubated for 2–4 h, and formazan crystals were dissolved in DMSO. Absorbance at 570 nm was measured, and IC_{50} values were calculated using GraphPad Prism [49].

Calculation:

- Calculate the percentage of cell viability and IC_{50} values.

$$\text{Cell viability \%} = \frac{\text{Sample}}{\text{Control}} \times 100$$

PPAR- γ Gene Expression Analysis By qRT-PCR: Gene expression analysis was done on 3T3-L1 cells treated with 3-AKBA (IC_{50} dose) or standard drug. RNA was extracted using TRIZOL, purified, DNase-treated, and reverse-transcribed into cDNA. qRT-PCR targeting PPAR-γ (with β-actin as control) was performed using SYBR Green on a QuantStudio 5 system. Data were analyzed by the 2^–ΔΔCt method, and melting curve confirmed specificity [50].

RESULTS

3.1. Network Pharmacology

SwissADME was used to identify 3-AKBA targets via its SMILES structure, focusing on Homo sapiens genes. Disease-associated genes were retrieved from DisGeNET. After removing duplicates, common targets were identified using InteractiVenn. STRING database provided PPI data, and Cytoscape was used to visualize the network and identify hub genes for molecular docking (Figure 6, 7, 8).

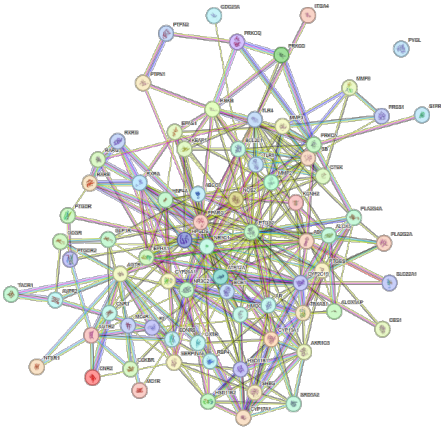

Figure 6: Disease gene

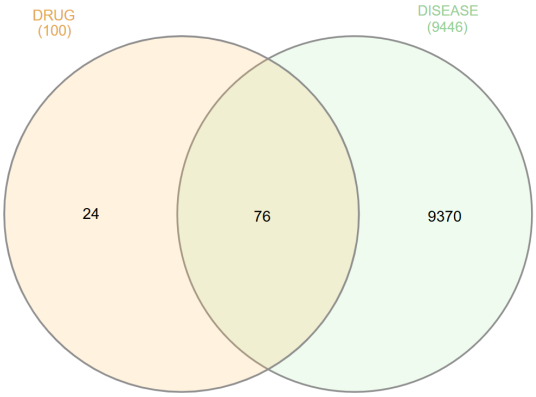

Figure 7: Venn diagram

Table 1: List of common target genes involved in PPAR-γ targeted HMGB1 Pathway.

	TARGETGENES	
ALOX5	PLA2G2A	PRKCQ
PTGES	PTGS2	AVPR2
HSD11B2	CCKBR	CYP26A1
HSD11B1	PTGDR	EPHX1

CYP17A1	HNF4A	MMP3
NR3C1	EPAS1	MMP2
BCL2L1	CYP19A1	MMP8
PTPN1	RXRA	KEAP1
AR	PRSS1	KCNH2
SERINA6	PTPN2	GLP1R
NR3C2	ALOX5AP	GCGR
F2	PRKCA	PYGL
SHBG	RXRG	PTGDR2
CDC25A	AGTR1	CES1
NOS2	ABCB1	RARG
IKBKB	TLR9	AGTR2
AKRIC3	OXTR	TBXAS1
HMGCR	RBP4	ABCC8
CYP2C19	EDNRB	ITGA4

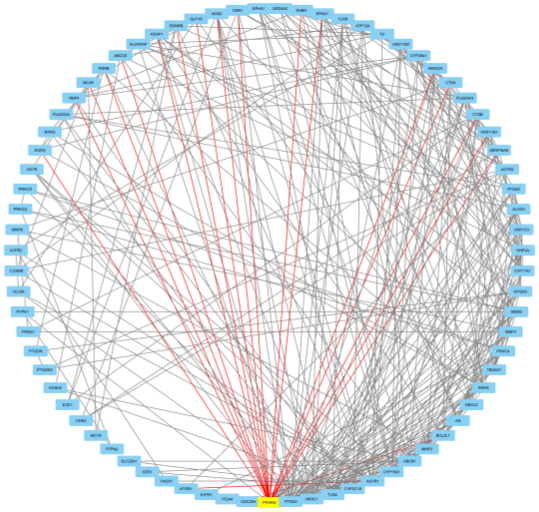

Figure 8: PPI Interaction

3.2. In Silico Studies

Molecular Docking: The MC4R shows highest binding score, which is -10.9 and shown in Table 2.

Table 2: Results of molecular docking studies.

SL.NO	GENE TARGET (PDB ID)	2D DOCKING INTERACTION	SCORE (kcal/mol)
1.	CNR1	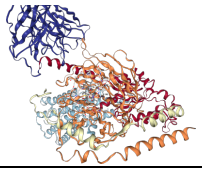	-8.9
2.	HMGCR		-8.3
3.	MC4R	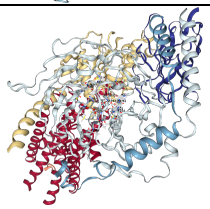	-10.9
4.	RBP4	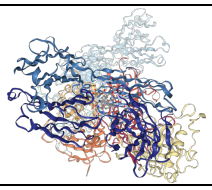	-8.6
5.	RXRB	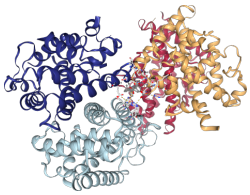	-9.5
6.	RXRG	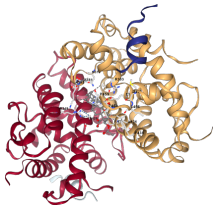	-7.8

Pharmacokinetics: Absorption, Distribution, Metabolism, Excretion and BBB permeability shown in Figure 9- 13. Pharmacokinetic analysis (via SwissADME and ADMET) shows 3-AKBA has high oral absorption (99.51%) but poor water solubility and low skin permeability. It is moderately permeable in the intestine, not a P-gp substrate but inhibits P-gp II. It binds strongly to plasma proteins, has low tissue distribution, and poor BBB penetration. Metabolized mainly by CYP3A4, with low clearance and non-renal excretion.

Property	Model Name	Predicted Value	Unit
Absorption	Water solubility	**-4.054**	Numeric (log mol/L)
Absorption	Caco2 permeability	**0.66**	Numeric (log Papp in 10^{-6} cm/s)
Absorption	Intestinal absorption (human)	**99.51**	Numeric (% Absorbed)
Absorption	Skin Permeability	**-2.735**	Numeric (log Kp)
Absorption	P-glycoprotein substrate	**No**	Categorical (Yes/No)
Absorption	P-glycoprotein I inhibitor	**No**	Categorical (Yes/No)
Absorption	P-glycoprotein II inhibitor	**Yes**	Categorical (Yes/No)

Fig 9: Absorption of 3-AKBA.

Distribution	VDss (human)	**-1.165**	Numeric (log L/kg)
Distribution	Fraction unbound (human)	**0**	Numeric (Fu)
Distribution	BBB permeability	**-0.113**	Numeric (log BB)
Distribution	CNS permeability	**-1.309**	Numeric (log PS)

Fig 10: Distribution of 3-AKBA.

Metabolism	CYP2D6 substrate	**No**	Categorical (Yes/No)
Metabolism	CYP3A4 substrate	**Yes**	Categorical (Yes/No)
Metabolism	CYP1A2 inhibitior	**No**	Categorical (Yes/No)
Metabolism	CYP2C19 inhibitior	**No**	Categorical (Yes/No)
Metabolism	CYP2C9 inhibitior	**No**	Categorical (Yes/No)
Metabolism	CYP2D6 inhibitior	**No**	Categorical (Yes/No)
Metabolism	CYP3A4 inhibitior	**No**	Categorical (Yes/No)

Fig 11: Metabolism of 3-AKBA

Excretion	Total Clearance	**-0.066**	Numeric (log ml/min/kg)
Excretion	Renal OCT2 substrate	**No**	Categorical (Yes/No)

Fig 12: Excretion of 3-AKBA.

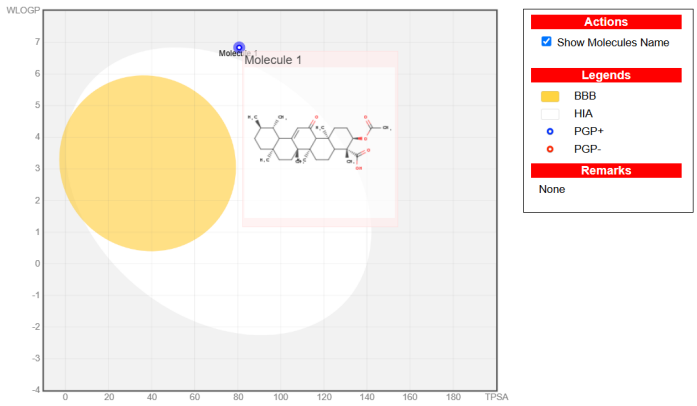

Fig 13: BBB permeability of 3-AKBA.

Toxicity: Prediction of Toxicity studies were done in Protox prediction software, shown in Figure 14.

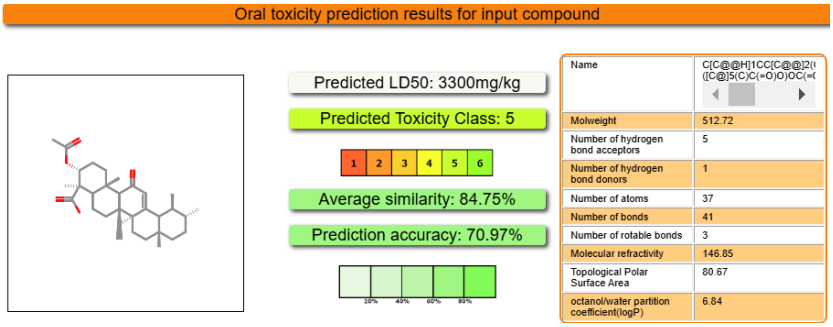

Fig 14: Toxicity prediction of 3-AKBA.

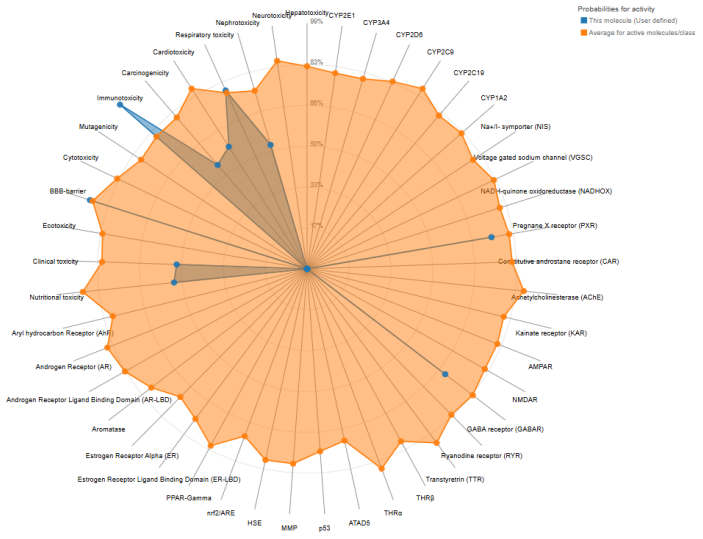

Fig 15: Radar plot analysis of 3-AKBA.

3-AKBA has low predicted oral toxicity (LD_{50}: 3300 mg/kg) and falls under Toxicity Class 5, indicating harm only at high doses. It shows high structural similarity (84.75%) and good prediction accuracy (70.97%) (Figure 14). Radar plot analysis indicates low risk of immunotoxicity, mutagenicity, cytotoxicity, and clinical toxicity, but moderate potential for carcinogenicity and hepatotoxicity, warranting further in vivo evaluation. (Figure 15)

Molecular dynamics: Predictions of molecular dynamic study were done in Schrondinger software.

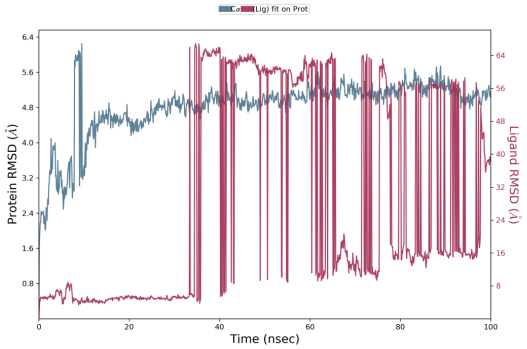

Fig 16: RMSD plot

The RMSD plot (Figure 16) indicates that the MC4R protein stabilizes after ~20 ns, maintaining an RMSD between 3.5–5.0 Å, suggesting structural stability.

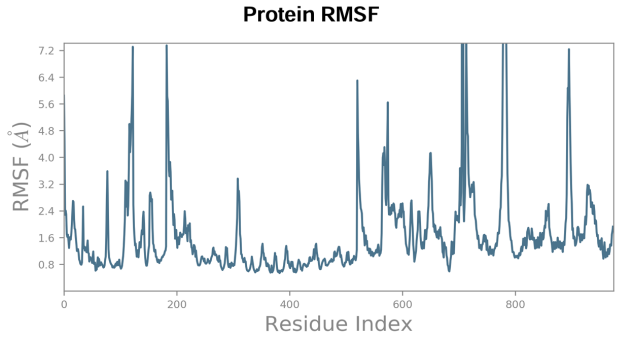

Fig 17: RMSF plot

The RMSF plot (Figure 17) shows flexible regions in the MC4R protein, with peaks indicating high fluctuation in loop regions, while stable regions exhibit lower RMSF values. These fluctuations help identify critical regions that may influence ligand binding and protein function.

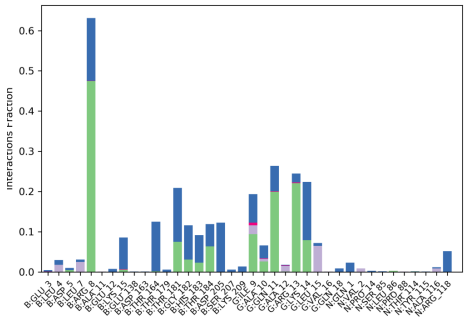

Fig 18: Interaction Histogram

The interaction histogram (Figure 18) reveals key binding residues, with stable interactions.

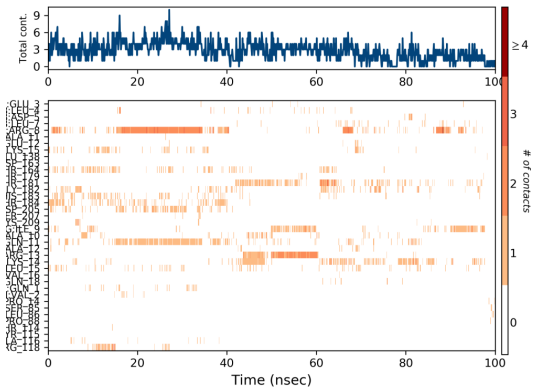

Fig 19: Contact Timeline

3-AKBA interacts with MC4R, its binding stability may require further optimization for improved efficacy (Figure 19).

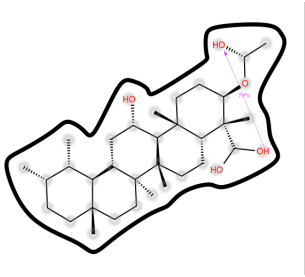

Fig 20: Ligand interaction

The ligand interaction map (Figure 20) shows key hydrogen bonds between 3-AKBA and MC4R with 79% occupancy, indicating strong and stable binding. Additional hydrogen and hydrophobic interactions highlight crucial functional groups involved, supporting the ligand's affinity and stability within the binding pocket.

3.3. HPLC Report

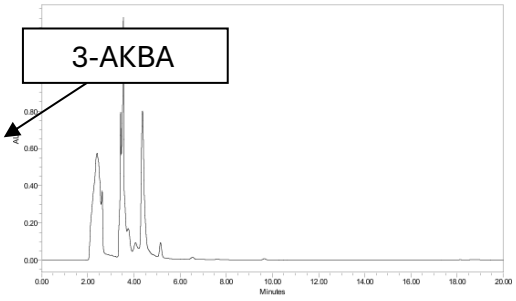

Fig 21: HPLC analysis of 3-AKBA.

The HPLC chromatogram of 3-AKBA (Figure 21), recorded at 260 nm, shows a main peak eluting between 3.5–4.2 minutes, indicating its presence and purity. The analysis used a 20 µL injection from vial 16 with a 20-minute run time. Sharp, well-resolved peaks confirm efficient separation and method suitability.

3.4. In-vitro Studies

3.4.1 Cytotoxicity Using Brine Shrimp Lethality Assay

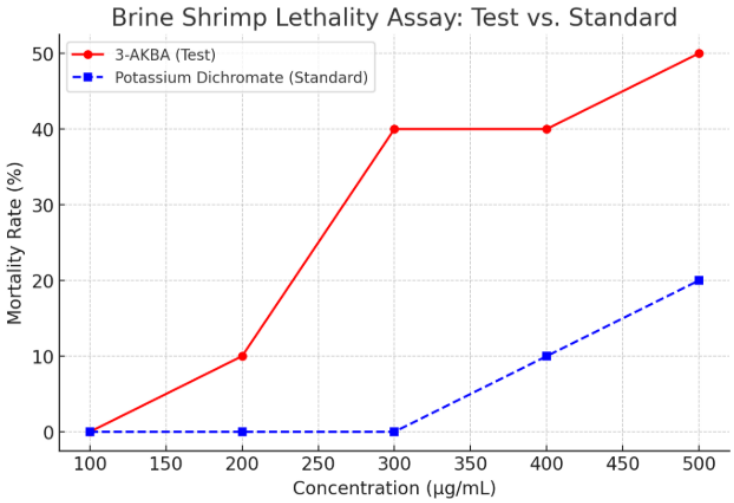

Fig 22: Brine shrimp lethality assay demonstrates concentration-dependent rise in the mortality rate.

The brine shrimp lethality assay showed an LC_{50} of 500 µg/mL for 3-AKBA, indicating 50% mortality at this concentration. Mortality increased with dose, suggesting dose-dependent cytotoxicity. In contrast, the standard (potassium dichromate) showed only 20% mortality at the highest dose, indicating lower toxicity. This suggests 3-AKBA may exhibit cytotoxic effects at higher concentrations.

3.4.2 Antioxidant Assay

DPPH:

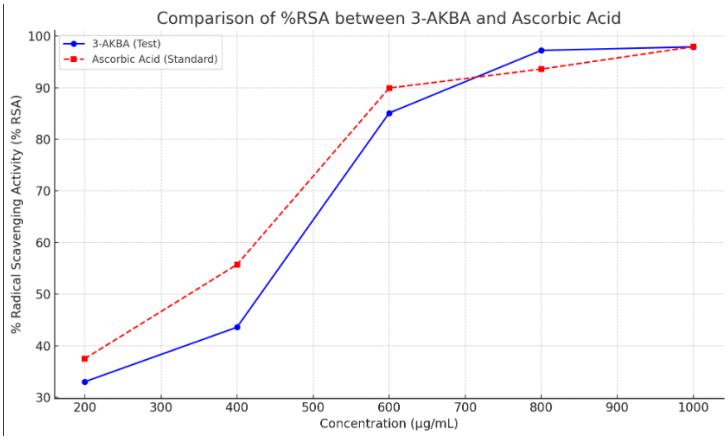

Fig 23: Comparison of %RSA of 3-AKBA and Ascorbic Acid.

The DPPH assay shows 3-AKBA has an IC_{50} of 433.91 µg/mL, compared to 371.46 µg/mL for ascorbic acid. Ascorbic acid shows higher %RSA at lower doses, but both exceed 85% RSA from 600 µg/mL onwards. At 800 µg/mL, 3-AKBA reaches 97.23% RSA, slightly surpassing ascorbic acid. At 1000 µg/mL, both approach ~98% RSA, indicating strong antioxidant potential of 3-AKBA at higher concentrations.

FRAP:

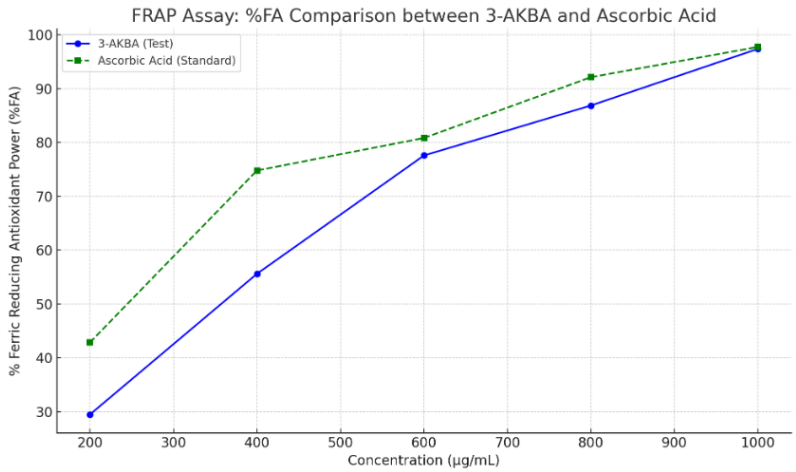

Fig 24: Comparison of %FA of 3-AKBA and Ascorbic Acid.

The FRAP assay shows IC_{50} values of 450.04 µg/mL for 3-AKBA and 272.16 µg/mL for ascorbic acid. Ascorbic acid exhibits stronger antioxidant activity at lower concentrations (200–400 µg/mL). However, 3-AKBA shows a sharp increase from 600 µg/mL, nearly matching ascorbic acid. At 1000 µg/mL, their %FA values are comparable (ascorbic acid: 97.76%, 3-AKBA: 97.39%), indicating that 3-AKBA has strong antioxidant potential at higher doses.

3.4.3 Anti-inflammatory using Protein Denaturation Method

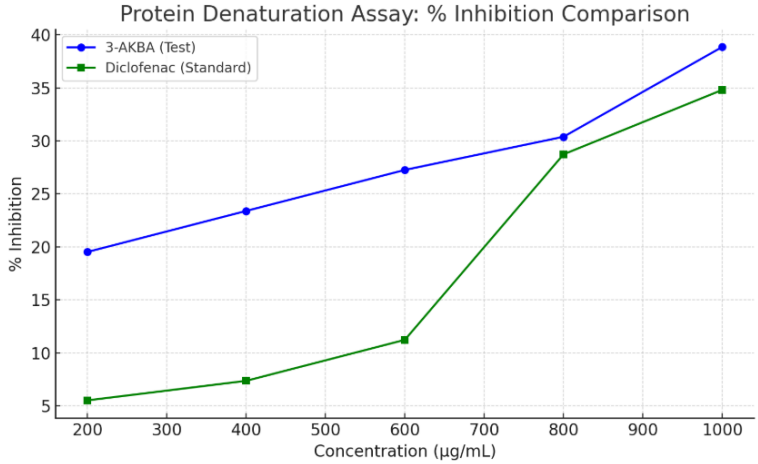

Fig 25: Comparing the Protein Denaturation inhibition activity of 3-AKBA and Diclofenac.

The protein denaturation assay shows IC_{50} values of 2722.52 µg/mL for 3-AKBA and 1307.28 µg/mL for diclofenac. 3-AKBA demonstrates higher % inhibition than diclofenac at lower doses (200–600 µg/mL), indicating stronger anti-inflammatory activity in that range. At 800 µg/mL, both show similar activity, peaking at 1000 µg/mL. These results suggest that 3-AKBA possesses notable anti-inflammatory potential, especially at lower concentrations.

3.4.4 Hyperglycaemic Studies

Alpha-Amylase Assay Using Iodine Starch Method:

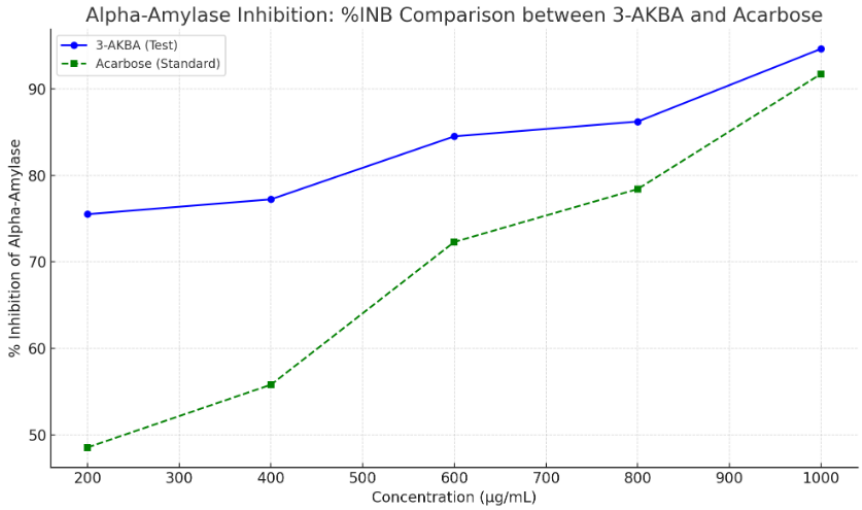

Fig 26: Comparing the Alpha-Amylase inhibitory activity of 3-AKBA and Acarbose.

The alpha-amylase inhibition assay shows that 3-AKBA has stronger, dose-dependent enzyme inhibition than Acarbose at all tested concentrations. At 1000 µg/mL, 3-AKBA achieves 94.658% inhibition vs. 91.756% for Acarbose. IC_{50} values are 1137.48 µg/mL for 3-AKBA and 828.40 µg/mL for Acarbose. These results suggest that 3-AKBA has significant alpha-amylase inhibitory potential, supporting its promise as an antidiabetic agent.

Alpha-Glucosidase Assay:

The α-glucosidase inhibition assay shows that 3-AKBA (IC_{50}: 388.52 µg/mL) and Acarbose (IC_{50}: 386.59 µg/mL) have nearly equal inhibitory potential. Both exhibit dose-dependent inhibition, but 3-AKBA consistently outperforms Acarbose across all concentrations. At 1000 µg/mL, 3-AKBA achieves 98.13% inhibition vs. 97.84% for Acarbose, indicating 3-AKBA's strong potential in controlling postprandial blood glucose spikes.

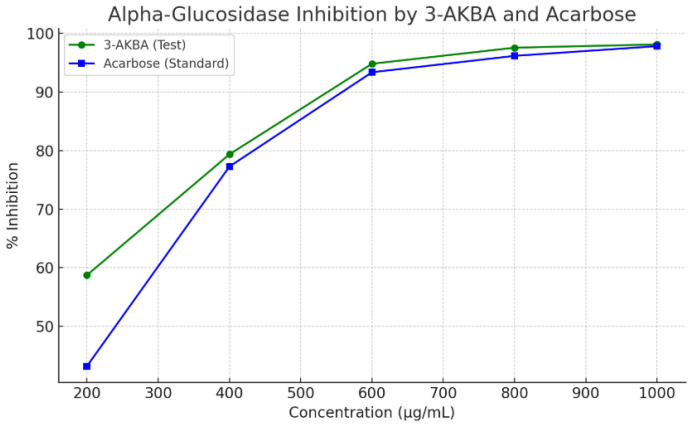

Fig 27: Comparing the Alpha-Glucosidase inhibitory activity of 3-AKBA and Acarbose.

Glucose Uptake Assay In Yeast Cells Using DNS:

Fig 28: Glucose Uptake inhibitory activity of 3-AKBA and Metformin.

The glucose uptake assay shows that 3-AKBA (IC_{50}: 190.03 µg/mL) has significantly stronger inhibitory activity than metformin (IC_{50}: 429.49 µg/mL). Both drugs show concentration-dependent glucose uptake inhibition, but 3-AKBA consistently outperforms metformin at all doses, reaching 97.54% inhibition at 1000 µg/mL. This indicates that 3-AKBA is a potent inhibitor of glucose absorption, highlighting its strong antidiabetic potential.

3.4.5 Cell Line Study

Cell Viability Using MTT Assay:

The MTT assay shows that 3-AKBA reduces cell viability in a dose-dependent manner, with an IC_{50} of 619.2 µg/mL compared to 496.9 µg/mL for pioglitazone.

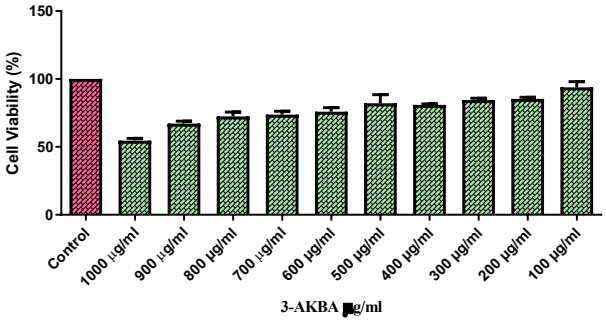

Fig 29: Cell Viability of 3-AKBA

The control group shows ~100% viability, while 3-AKBA-treated cells show decreasing viability with increasing dose, remaining above 50% even at 1000 µg/mL. This suggests 3-AKBA has moderate cytotoxicity and retains good cell viability at lower concentrations, supporting its potential for safe therapeutic use.

Fig 30: Control and Treated cell of 3-AKBA at various concentrations.

CONC.	IMAGE
CONTROL	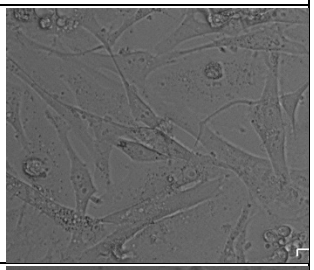
1000 µg/ml	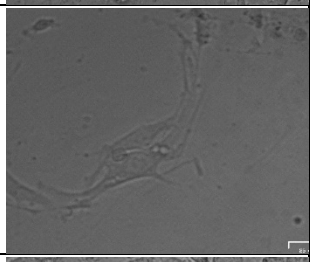
900 µg/ml	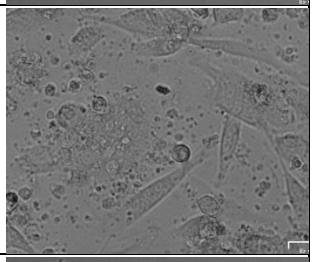
800 µg/ml	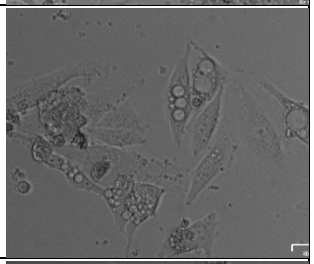
700 µg/ml	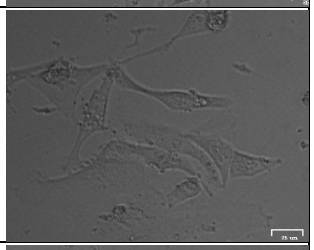
600 µg/ml	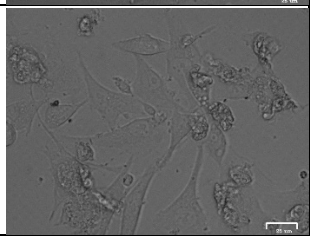

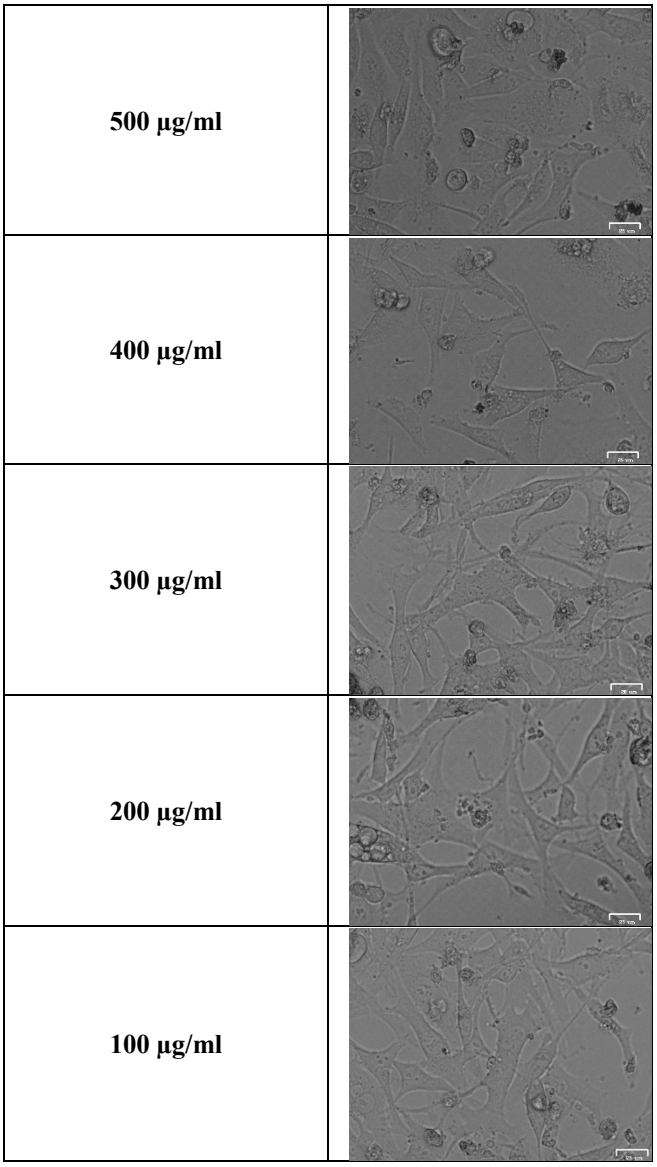

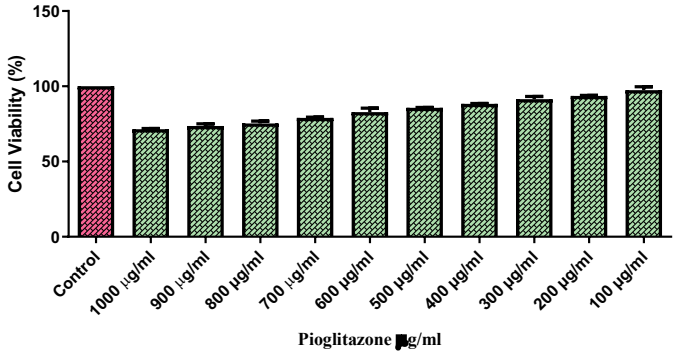

Fig 31: Cell Viability of Pioglitazone

The bar graph shows that Pioglitazone causes a mild, dose-dependent decrease in cell viability, with an IC_{50} of 496.9 µg/mL. The control group maintains ~100% viability, while the highest concentration (1000 µg/mL) reduces viability to ~50%. Lower concentrations (100–900 µg/mL) preserve high viability, indicating minimal cytotoxicity and suggesting Pioglitazone is generally safe at therapeutic doses.

Fig 32: Control and Treated cell of Pioglitazone at various concentrations.

CONC.	IMAGE
CONTROL	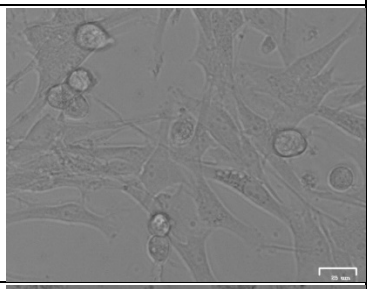
1000 µg/ml	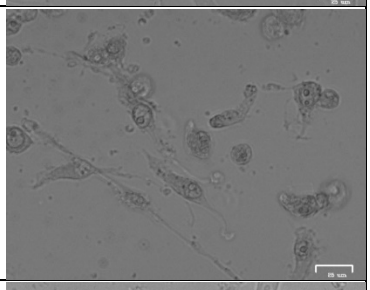
900 µg/ml	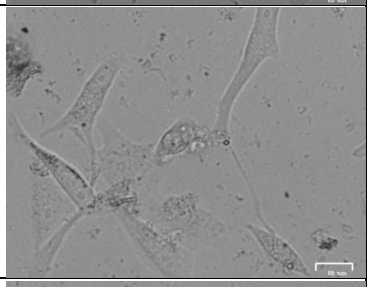
800 µg/ml	
700 µg/ml	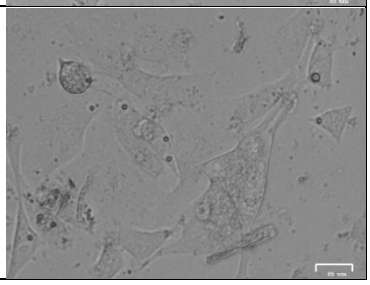

600 µg/ml	
500 µg/ml	
400 µg/ml	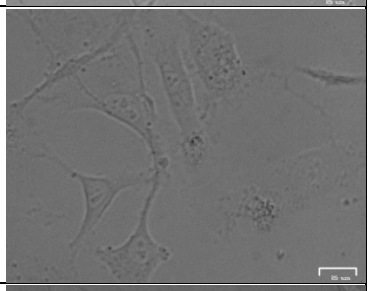
300 µg/ml	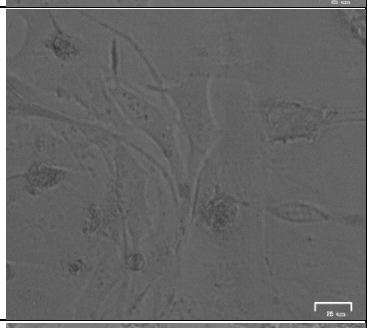
200 µg/ml	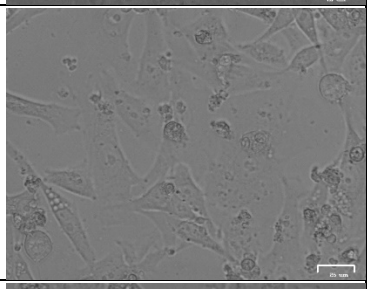
100 µg/ml	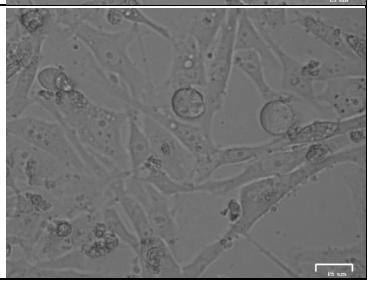

PPAR- γ Gene Expression Analysis By qRT-PCR:

Results Summary

Sample	Target	Cт Mean	Cт SD	ΔCт Mean	ΔCт SD Err	ΔΔCт	RQ	RQ Min	RQ Max
3-AKBA	B-actin†	32.202	1.405						
Control*	B-actin†	32.549	0.586						
STD	B-actin†	32.210	1.364						
3-AKBA	PPAR-G	29.945	1.733	-2.257	1.288	-1.570	2.969	0.249	35.415
Control*	PPAR-G	31.862	0.535	-0.687	0.458	0.000	1.000	0.414	2.415
STD	PPAR-G	30.758	0.529	-1.452	0.845	-0.765	1.699	0.334	8.637

Fig 33: PPAR-γ expression Analysis

The data indicates that 3-AKBA significantly upregulates PPAR-γ expression (RQ = 2.969) compared to pioglitazone (RQ = 1.699), highlighting its stronger potential to modulate inflammation. Given PPAR-γ's key role in anti-inflammatory pathways, 3-AKBA shows promise as a potent candidate for anti-inflammatory therapy.

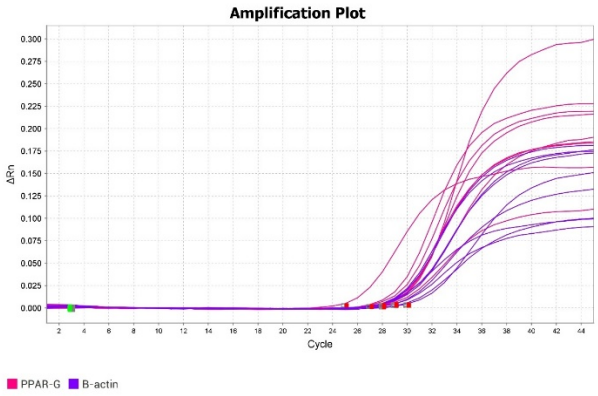

Fig 34: Amplification plot

The amplification plot shows earlier Ct values for PPAR-γ (pink curves) in 3-AKBA-treated samples compared to pioglitazone and control, indicating higher gene expression. β-actin (purple curves) remains consistent across all groups, confirming reliable normalization. This earlier and stronger amplification of PPAR-γ supports that 3-AKBA more effectively enhances its expression, reinforcing its potential as a potent anti-inflammatory agent through PPAR-γ activation.

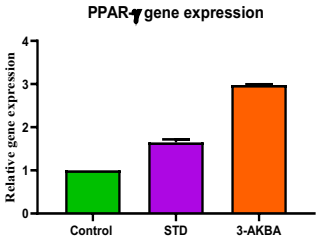

Fig 35: Bar plot

The bar graph demonstrates a significant upregulation of PPAR-γ expression in the 3-AKBA-treated group compared to both control and pioglitazone (STD) groups. While pioglitazone shows moderate activation, 3-AKBA induces a markedly stronger effect, indicating its superior potential to activate PPAR-γ-mediated anti-inflammatory pathways. This supports 3-AKBA as a promising and potent anti-inflammatory agent.

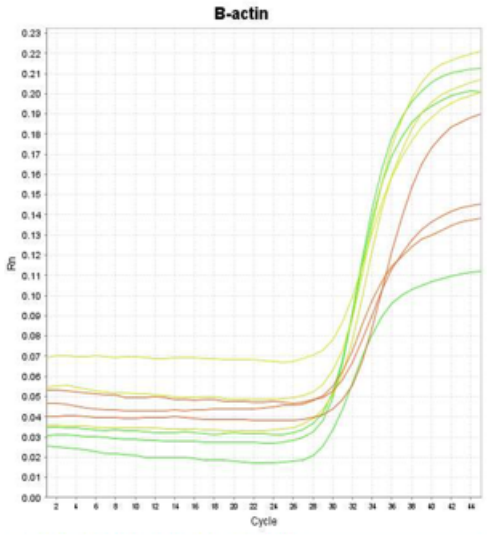

Fig 36: Amplification plot for B-actin

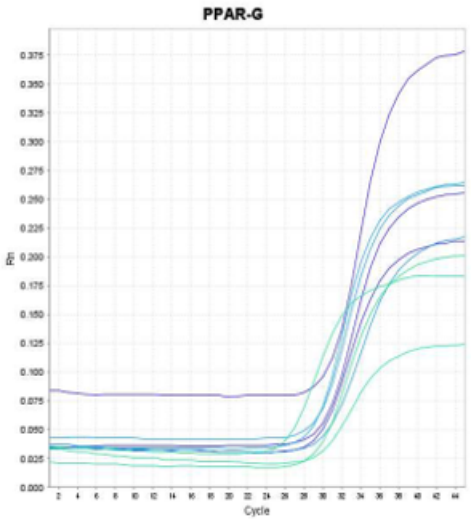

Fig 37: Amplification plot of PPAR-γ

The amplification plots (Figure 32 and 33) show consistent Ct values for B-actin across all samples, confirming proper normalization. PPAR-γ amplifies earlier in the 3-AKBA-treated group compared to pioglitazone and control, indicating significantly higher expression. This suggests that 3-AKBA strongly upregulates PPAR-γ, reinforcing its potential as a more effective anti-inflammatory agent.

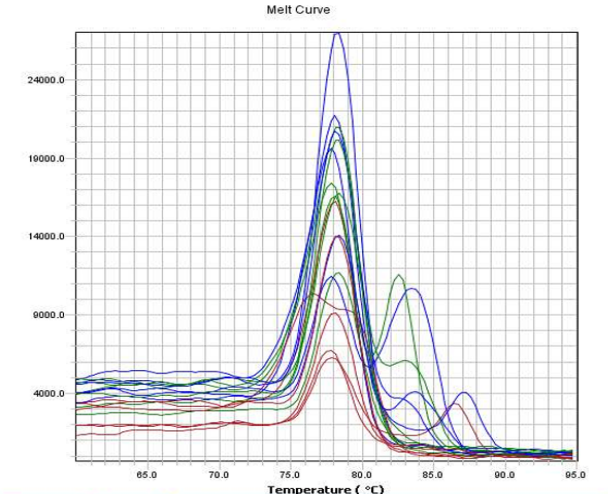

Fig 38: Melt curve analysis

The melt curve analysis shows a single sharp peak for each sample, confirming specific amplification of PPAR-γ without primer-dimers or non-specific products. Consistent peak temperatures across samples validate the qRT-PCR results, ensuring the observed PPAR-γ upregulation in 3-AKBA-treated cells is accurate. This reinforces the reliability of the data and supports 3-AKBA's strong potential as an anti-inflammatory agent.

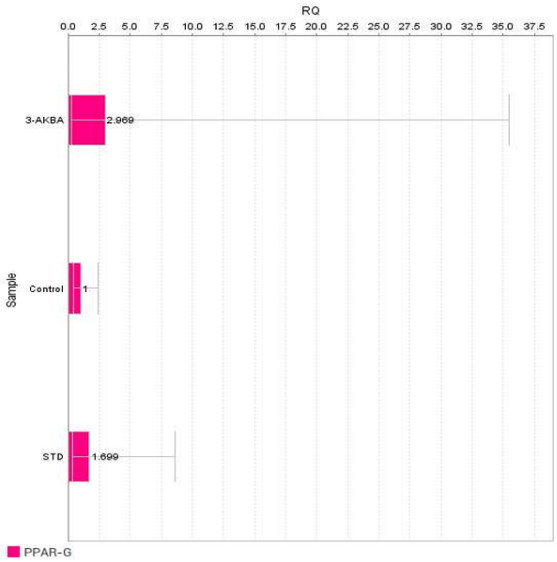

Fig 39: RQ plot

The relative quantification (RQ) plot indicates that PPAR-γ expression is significantly upregulated in the 3-AKBA-treated group (RQ = 2.969) compared to the control (RQ = 1) and standard Pioglitazone (RQ = 1.699). This suggests that 3-AKBA enhances PPAR-γ expression more effectively than Pioglitazone, reinforcing its potential as a stronger anti-inflammatory agent via PPAR-γ activation.

DISCUSSION

his study explored the neuroprotective potential of 3-AKBA in diabetes-induced Alzheimer's disease (AD), focusing on its effects via PPARγ activation and the HMGB1 signaling pathway. Using network pharmacology, in silico docking, and in vitro experiments, the compound demonstrated significant anti-inflammatory, antioxidant, and glucose-modulatory properties.

Diabetes and AD share common mechanisms such as chronic hyperglycemia, insulin resistance, and neuroinflammation. The study highlighted HMGB1 as a key mediator, upregulated in both conditions, and identified it as a central node in the protein interaction network. HMGB1 promotes inflammation through TLR and RAGE activation, making it a valuable therapeutic target.

3-AKBA, a bioactive compound from Boswellia serrata, showed good purity through HPLC analysis and strong binding to PPARγ in docking studies. Molecular simulations suggested it may act as a partial agonist of PPARγ, which plays a vital role in reducing inflammation and improving insulin sensitivity by downregulating NF-κB.

Experimental findings supported these results. Antioxidant assays (DPPH, FRAP) confirmed high radical scavenging activity. The protein denaturation assay showed anti-inflammatory potential, while enzyme inhibition studies demonstrated significant α-amylase and α-glucosidase inhibition, indicating antidiabetic potential. Brine shrimp assay showed low cytotoxicity, and MTT assays suggested dose-dependent but manageable toxicity at therapeutic levels.

Finally, in 3T3-L1 adipocytes, 3-AKBA significantly upregulated PPARγ expression, as confirmed by qRT-PCR. These results suggest that 3-AKBA mitigates neuroinflammation in diabetes-linked AD through HMGB1-PPARγ modulation, supporting its potential as a therapeutic candidate in managing neurodegeneration and metabolic dysfunction.

CONCLUSION

This study highlights the promising neuroprotective role of 3-AKBA in diabetes-induced Alzheimer's disease by targeting the HMGB1-PPARγ signaling pathway. Through integrated network pharmacology, *in silico* modeling, and gene expression analysis, 3-AKBA demonstrated potent anti-inflammatory, antioxidant, and glucose-regulating properties. The compound significantly upregulated PPARγ expression while downregulating HMGB1-associated inflammatory genes, suggesting its effectiveness in modulating neuroinflammation via the gut-brain axis. The findings underscore 3-AKBA's potential as a multifunctional therapeutic agent capable of addressing the intertwined pathologies of metabolic dysfunction and neurodegeneration.

FUTURE PERSPECTIVE

Future research should focus on validating the therapeutic potential of 3-AKBA through in vivo studies to assess its pharmacokinetics, bioavailability, and long-term safety in diabetes-induced Alzheimer’s models. Exploring advanced drug delivery systems like nanoparticles may enhance its brain-targeted delivery and stability. Additionally, investigating its interaction with other molecular pathways such as SIRT1, AMPK, and MAPK could provide deeper insight into its multi-target actions. Early-phase clinical trials are essential to evaluate its efficacy and safety in humans. Overall, 3-AKBA holds promise as a novel therapeutic agent for managing diabetes-associated neuroinflammation and cognitive decline.

REFERENCES

1. Kitabchi AE, Umpierrez GE, Miles JM, Fisher JN. Hyperglycemic crises in adult patients with diabetes. Diabetes Care. 2009, 32:1335-43. 10.2337/dc09-9032.
2. Schachter AS, Davis KL: Alzheimer's disease. Dialogues Clin Neurosci. 2000, 2:91-100. 10.31887/DCNS.2000.2.2/asschachter.
3. Kukull WA, Higdon R, Bowen JD, et al. Dementia and Alzheimer disease incidence: a prospective cohort study. Arch Neurol. 2002, 59:1737-46. 10.1001/archneur.59.11.1737.
4. Tahapary DL, Pratisthita LB, Fitri NA, et al. Challenges in the diagnosis of insulin resistance: focusing on the role of HOMA-IR and tryglyceride/glucose index. Diabetes Metab Syndr. 2022, 16:102581. 10.1016/j.dsx.2022.102581.
5. Vidal-Ostos F, Ramos-Lopez O, Blaak EE, Astrup A, Martinez JA. The triglyceride-glucose index as an adiposity marker and a predictor of fat loss induced by a low-calorie diet. Eur J Clin Invest. 2022, 52:e13674. 10.1111/eci.13674.
6. Wortwein G, Gustafson B, Hansen KL, Mogensen J. Behavioral symptoms in adult rats after postnatal l-nitro-arginine. Int J Dev Neurosci. 1997, 15:147-54. 10.1016/S0736-5748(97)00002-6.
7. Ferreira D, Perestelo-Pérez L, Westman E, Wahlund LO, Sarría A, Serrano-Aguilar P. Meta-review of CSF core biomarkers in Alzheimer's disease: the state-of-the-art after the new revised diagnostic criteria. Front Aging Neurosci. 2014, 6:47. 10.3389/fnagi.2014.00047.
8. Petersen RC, Lopez O, Armstrong MJ, et al. Practice guideline update summary: mild cognitive impairment: report of the Guideline Development, Dissemination, and Implementation Subcommittee of the American Academy of Neurology. Neurology. 2018, 90:126-35. 10.1212/WNL.0000000000004826.
9. Mudher A, Lovestone S. Alzheimer's disease - do tauists and baptists finally shake hands. Trends Neurosci. 2002, 25:22-6. 10.1016/S0166-2236(00)02031-2.
10. Rajaei E, Jalali MT, Shahrabi S, Asnafi AA, Pezeshki SM. HLAs in autoimmune diseases: dependable diagnostic biomarkers?. Curr Rheumatol Rev. 2019, 15:269-76. 10.2174/1573397115666190115143226.
11. Jenkins TA, Nguyen JC, Polglaze KE, Bertrand PP. Influence of tryptophan and serotonin on mood and cognition with a possible role of the gut-brain axis. Nutrients. 2016, 8:56. 10.3390/nu8010056.
12. Strandwitz P. Neurotransmitter modulation by the gut microbiota. Brain Res. 2018, 1693:128-33. 10.1016/j.brainres.2018.03.015.
13. Worthington JJ, Reimann F, Gribble FM. Enteroendocrine cells-sensory sentinels of the intestinal environment and orchestrators of mucosal immunity. Mucosal Immunol. 2018, 11:3-20. 10.1038/mi.2017.73.
14. Sgritta M, Dooling SW, Buffington SA, Momin EN, Francis MB, Britton RA, Costa-Mattioli M. Mechanisms underlying microbial-mediated changes in social behavior in mouse models of autism spectrum disorder. Neuron. 2019, 101:246-59.e6. 10.1016/j.neuron.2018.11.018.
15. Krieger JP, Asker M, van der Velden P, et al. Neural pathway for gut feelings: vagal interoceptive feedback from the gastrointestinal tract is a critical modulator of anxiety-like behavior. Biol Psychiatry. 2022, 92:709-21. 10.1016/j.biopsych.2022.04.020.
16. MahmoudianDehkordi S, Arnold M, Nho K, et al. Altered bile acid profile associates with cognitive impairment in Alzheimer's disease-an emerging role for gut microbiome. Alzheimers Dement. 2019, 15:76-92. 10.1016/j.jalz.2018.07.217.
17. Jenkins TA, Nguyen JC, Polglaze KE, Bertrand PP. Influence of tryptophan and serotonin on mood and cognition with a possible role of the gut-brain axis. Nutrients. 2016, 8:56. 10.3390/nu8010056.
18. Fülling C, Dinan TG, Cryan JF. Gut microbe to brain signaling: what happens in vagus…. Neuron. 2019, 101:998-1002. 10.1016/j.neuron.2019.02.008.

19. Mandke P, Vasquez KM. Interactions of high mobility group box protein 1 (HMGB1) with nucleic acids: implications in DNA repair and immune responses. DNA Repair (Amst). 2019, 83:102701. 10.1016/j.dnarep.2019.102701.
20. Martinotti S, Patrone M, Ranzato E. Emerging roles for HMGB1 protein in immunity, inflammation, and cancer. Immunotargets Ther. 2015, 4:101-9. 10.2147/ITT.S58064
21. Xue J, Suarez JS, Minaai M, et al. HMGB1 as a therapeutic target in disease. J Cell Physiol. 2021, 236:3406-19. 10.1002/jcp.30125.
22. Paudel YN, Shaikh MF, Chakraborti A, et al. HMGB1: a common biomarker and potential target for TBI, neuroinflammation, epilepsy, and cognitive dysfunction. Front Neurosci. 2018, 12:628. 10.3389/fnins.2018.00628.
23. Le Page A, Dupuis G, Frost EH, Larbi A, Pawelec G, Witkowski JM, Fulop T. Role of the peripheral innate immune system in the development of Alzheimer's disease. Exp Gerontol. 2018, 107:59-66. 10.1016/j.exger.2017.12.019.
24. Nan K, Han Y, Fang Q, et al. HMGB1 gene silencing inhibits neuroinflammation via down-regulation of NF-κB signaling in primary hippocampal neurons induced by Aβ25-35. Int Immunopharmacol. 2019, 67:294-301. 10.1016/j.intimp.2018.12.027.
25. Chinetti G, Fruchart JC, Staels B. Peroxisome proliferator-activated receptors and inflammation: from basic science to clinical applications. International Journal of Obesity. 2003, 27(supplement 3):S41–S45. 10.1038/sj.ijo.0802357.
26. Harmon GS, Lam MT, Glass CK. PPARs and lipid ligands in inflammation and metabolism. Chemical Reviews. 2011, 111(10):6321–6340. 10.1021/cr2001355.
27. Blanquart C, Barbier O, Fruchart JC, Staels B, Glineur C. Peroxisome proliferator-activated receptors: regulation of transcriptional activities and roles in inflammation. Journal of Steroid Biochemistry and Molecular Biology. 2003, 85(2–5):267–273. 10.1016/s0960-0760(03)00214-0.
28. Olefsky JM, Glass CK. Macrophages, inflammation, and insulin resistance. Annual Review of Physiology. 2009, 72:219–246. 10.1146/annurev-physiol-021909-135846.
29. Banno N, et al. Anti-inflammatory activities of the triterpene acids from the resin of Boswellia carteri. J Ethnopharmacol. 2006, 107, 249–253 . 10.1016/j.jep.2006.03.006.
30. Chen M, Wang M, Yang Q, Wang M, Wang Z, Zhu Y, Zhang Y, Wang C, Jia Y, Li Y., and Wen A. Antioxidant effects of hydroxysafflor yellow a and acetyl-11-keto-β-boswellic acid in combination on isoproterenol-induced myocardial injury in rats, International Journal of Molecular Medicine. 2016, 37, no. 6, 1501–1510. 10.3892/ijmm.2016.2571, 2-s2.0-84978805724.
31. Marefati N, Beheshti F, Vafaee F, Barabadi M, Hosseini M. The effects of incensole acetate on neuro-inflammation, brain-derived neurotrophic factor and memory impairment induced by lipopolysaccharide in rats, Neurochemical Research. 2021, 46, no. 9, 2473–2484. 10.1007/s11064-021-03381-3.
32. Marefati N, Beheshti F, Mokhtari-Zaer A, Shafei MN, Salmani H, Sadeghnia HR, Hosseini M. The effects of olibanum on oxidative stress indicators, cytokines, brain derived neurotrophic factor and memory in lipopolysaccharide challenged rats, Toxin Reviews. 2020, 1–14. 10.1080/15569543.2020.
33. Marefati N, Beheshti F, Memarpour S, Bayat R, Naser Shafei M, Sadeghnia HR, Ghazavi H, Hosseini M. The effects of acetyl-11-keto-β-boswellic acid on brain cytokines and memory impairment induced by lipopolysaccharide in rats, Cytokine. 2020, 131, 155107. 10.1016/j.cyto.2020.1551.
34. Marefati N, Khamse S, Khamse S, Mansouri S, Hosseini M, Anaeigoudari A. Effects of boswellia serrata resin on central nervous system: a mini review, Physiology and Pharmacology. 2021, 25, no. 4, 288–295. 10.52547/phypha.25.4.5.
35. Li W, Liu J, Fu W, Zheng X, Ren L, Liu S, Wang J, Ji T, Du G. 3-O-acetyl-11-keto-β-boswellic acid exerts anti-tumor effects in glioblastoma by arresting cell cycle at G2/M phase, Journal of Experimental & Clinical Cancer Research. 2018, 37, no. 1. 10.1186/s13046-018-0805-4, 2-s2.0-85049438591.
36. Iram F, Khan SA, Husain A. Phytochemistry and potential therapeutic actions of boswellic acids: a mini-review, Asian Pacific Journal of Tropical Biomedicine. (2017) 7, no. 6, 513–523. 10.1016/j.apjtb.2017.05.001, 2-s2.0-85020285843.

37. Marefati N, Beheshti F, Etemadizadeh P, Hosseini M, Anaeigoudari A. Gum resin extract of Boswellia serrata attenuates lipopolysaccharide-induced inflammation and oxidative damage in hepatic and renal tissues of rats, Asian Pacific Journal of Tropical Biomedicine. 2022, 12, no. 1, 20–25. 10.4103/2221-1691.333210
38. Al-Dhubiab BE, Patel SS, Morsy MA, Duvva H, Nair AB, Deb PK, Shah J. The beneficial effect of boswellic acid on bone metabolism and possible mechanisms of action in experimental osteoporosis, Nutrients. 2020, 12, no. 10. 10.3390/nu12103186.
39. Wei C, Fan J, Sun X, Yao J, Guo Y, Zhou B, Shang Y. Acetyl-11-keto-β-boswellic acid ameliorates cognitive deficits and reduces amyloid-β levels in APPswe/PS1dE9 mice through antioxidant and anti-inflammatory pathways. Free Radical Biology and Medicine. 2020, 150, 96-108. 10.1016/j.freeradbiomed.2020.02.022.
40. Gomaa AA, Farghaly HA, Abdel-Wadood YA, Gomaa GA. Potential therapeutic effects of boswellic acids/Boswellia serrata extract in the prevention and therapy of type 2 diabetes and Alzheimer’s disease. Naunyn-Schmiedeberg's Archives of Pharmacology. 2021, 1-19. 10.1007/s00210-021-02154-7.
41. Meyer BN, Ferrigni NR, Putnam JE, Jacobsen LB, Nichols DE, McLaughlin JL. Brine shrimp: A convenient general bioassay for active plant constituents. Planta Med. 1982, 45:31–4. 10.1055/s-2007-971236.
42. Sahgal G, Ramanathan S, Sasidharan S, Mordi MN, Ismail S, Mansor SM. Brine shrimp lethality and acute oral toxicity studies on Swietenia mahagoni (Linn.) Jacq. seed methanolic extract. Pharmacognosy research. 2010, Jul;2(4):215. 10.4103/0974-8490.69107.
43. Gulcin I. Antioxidants and antioxidant methods: An updated overview. Archives of toxicology. 2020, 94(3), 651-715. 10.1007/s00204-020-02689-3.
44. Soural I, Svestkova P, Hic P, Balik J. Different values obtained by the FRAP method for the determination of slowly and rapidly reacting phenols. Acta Alimentaria. 2022, Feb 28;51(1):84-92. 10.1556/066.2021.00168.
45. Dharmadeva S, Galgamuwa LS, Prasadinie C, Kumarasinghe N. In vitro anti-inflammatory activity of Ficus racemosa L. bark using albumin denaturation method. AYU (An international quarterly journal of research in Ayurveda). 2018, Oct 1;39(4):239-42. 10.4103/ayu.AYU_27_18.
46. Agatonovic-Kustrin S, Morton DW. HPTLC–Bioautographic methods for selective detection of the antioxidant and a-amylase inhibitory activity in plant extracts. MethodsX. 2018, Jan 1;5:797-802. 10.1016/j.mex.2018.07.013.
47. Daou M, Elnaker NA, Ochsenkühn MA, Amin SA, Yousef AF, Yousef LF. In vitro α-glucosidase inhibitory activity of Tamarix nilotica shoot extracts and fractions. Plos one. 2022 Mar 14;17(3):e0264969. 10.1371/journal.pone.0264969.
48. Pitchaipillai R, Ponniah T. In vitro antidiabetic activity of ethanolic leaf extract of bruguiera Cylindrica L.–glucose uptake by yeast cells method. International Biological and Biomedical Journal. 2016, Dec 10;2(4):171-5. http://ibbj.org/article-1-92-en.html.
49. Huang L, Huang QY, Huang HQ. The evidence of HeLa cell apoptosis induced with tetraethylammonium using proteomics and various analytical methods. The Journal of biological chemistry. 2014, 289(4), 2217–2229.
50. B. Usharani R, Monisha. In-vitro Cytotoxicity assay of Betel quid extract against HeLa cells. Research Journal of Pharmacy and Technology. 2022, 15(1):47-0.